Hyungsoon Park
Youn-sik Park
Center for Noise and Vibration Control
Department of Mechanical Engineering
Korea Advanced Institute of Science and Technology
Science Town, Taejon 305-701, Korea

Transient Response of an Impacted Beam and Indirect Impact Force Identification Using Strain Measurements

The impulse response functions (force–strain relations) for Euler–Bernoulli and Timoshenko beams are considered. The response of a beam to a transverse impact force, including reflection at the boundary, is obtained with the convolution approach using the impulse response function obtained by a Laplace transform and a numerical scheme. Using this relation, the impact force history is determined in the time domain and results are compared with those of Hertz's contact law. In the case of an arbitrary impact, the location of the impact force and the time history of the impact force can be found. In order to verify the proposed algorithm, measurements were taken using an impact hammer and a drop test of a steel ball. These results are compared with simulated ones. © *1994 John Wiley & Sons, Inc.*

INTRODUCTION

Impact is defined as a force of short duration acting on a structure; this causes a local response in the system. Impacts occur in many solid structures such as machines, link mechanisms, impact dampers, rotating blades, and structures that have internal gaps in a joint or an external impact source. In order to understand the characteristics of the impact and to find the impact force, which is generally difficult to measure, it is necessary to analyze the response of the impacted system at the exact instant of impact.

The impact beam problem as shown in Fig. 1 is widely used to examine the impact phenomenon. Frequently, the impact problem of a steel ball on a beam of infinite length is examined with Euler–Bernoulli beam theory. If a steel ball collides with a beam with velocity v_0, Euler–Bernoulli beam theory provides reasonable velocity and displacement solutions but gives an infinite strain at the instant of impact. At intuitive explanation for this is that the slope of the beam at the point of loading must be continuous and at the moment of impact a ball engages a finite portion of the beam; this is closely connected with the infinite wave velocity. On this basis, it is clear that a useful estimate of the initial strain can be obtained if wave propagation effects in the beam are included. Many studies have been done to calculate the response of the beam using a normal mode approach (Yamamoto, Sato, and Koseki, 1990) or infinite beam theory (Doyle, 1984a; McGhie, 1990; Stadler and Shreeves, 1970) using Hertz's contact theory (Willis, 1966), which is elastic contact law for a static case. The impact force, which is applied suddenly, causes plastic deformation at the center of the contact zone even for a small load (Cawley and Clayton, 1987) and generates a stress wave in the im-

Received July 14, 1993; accepted August 20, 1993.
Shock and Vibration, Vol. 1, No. 3, pp. 267–278 (1994)

CCC 1070-9622/94/030267-12

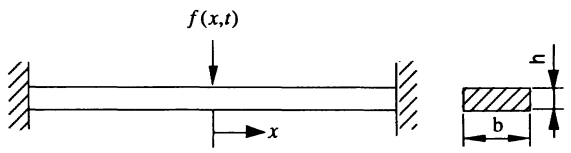

Length=1.0m Height, h=5.0mm
Width, b=25mm Poisson ratio, ν =0.3
Density, ρ =7800kg/m^3 Young's modulus, E =200GPa

FIGURE 1 Clamped beam for impact analysis.

pacted medium. That is to say, it takes a finite time for the effects of force to be felt at another point of the structure. The time duration of the impact process is so short that the resulting response has local behavior, and the standing wave cannot be fully developed in the early period of the impact. In this case, the normal mode approach is not appropriate. Some research has been done to obtain the response of a beam using the wave propagation approach in the frequency domain (Doyle and Kamle, 1985, 1987; Leung and Dinnington, 1990, 1992; Rizzi and Doyle, 1992). This approach has the advantage of simulating the propagation from one point to another, but cannot be used to calculate the response for a given force contact model, which is, in general, nonlinear. Thus, if we consider the wave propagation method in the time domain to analyze the impacted beam, we can obtain the initial response of the beam. The solution of the wave propagation method is useful for determining the initial response of the beam, and the subsequent response can be better obtained from a normal mode approach. The wave propagation method may have a narrow field of practical application but there are cases in which it is of value, such as the determination of the initial response of the system in this type of problem.

Many cases also arise in practice in which it is necessary to know the dynamic impact force where it is not possible to instrument the impactor. Chang and Sun (1989) used the impulse response function obtained from experiments and Doyle (1984b, 1987, 1991) used a frequency domain approach. Some research has been done to calculate the impact force from a measured acceleration by using rigid body acceleration (Batemann and Carne 1991, 1992) and by using the velocity by integrating the measured signal (Hollandsworth and Busby, 1989). Impact force is regarded as a point source in the sense that the dimensions of the source are small compared to the wavelength of interest. Thus, for both response and force analysis, the impulse response function of the beam is essential. Using the impulse response function, the response and impact force can be obtained with a convolution and deconvolution approach.

This article focuses on the transverse impact of a beam (Fig. 1) to investigate features of wave phenomena and to reconstruct the impact force from a measured strain signal using the impulse response function. In order to execute both response and force analysis, the impulse response function, which is the relationship between the force and strain, is obtained by using the wave propagation approach in the time domain. The Timoshenko beam equation, which shows more physically acceptable results in wave concepts, is solved using the Laplace transformation and numerical techniques. These results are compared with those from an Euler–Bernoulli beam model (McGhie, 1990). The impact force is then identified in the time domain using these results. For the analysis of an arbitrary impact, a numerical algorithm to find the position and the shape of the impact is also suggested. Simulation and experimental results are presented. In order to verify the validity of the suggested method, the identified impact force is compared with the directly measured value. Results show that the inversely reconstructed impact force matches measured value quite well in terms of peak, time to peak, and pulse duration. Impacts on the beam by a steel ball are tested and the reconstructed forces are compared with the results found using Hertz's contact law. Some limitations of Hertzian theory are discussed.

RESPONSE OF AN IMPACTED BEAM

The impact problem on a clamped beam as shown in Fig. 1 is first considered in this study. When an impact force generates stress waves in the beam, it takes a finite time to feel the effects of the loading at another position in the beam. The response of an impacted beam at the point not on a boundary is independent of the boundary conditions at the moment of impact. Therefore, it can be considered that the impacted beam behaves similarly to an infinite beam. Thus, the impulse response function of an infinite beam can be derived by using a Laplace transform to analyze the transverse impact on the beam.

The equation of motion of an infinite Euler–

Bernoulli beam is

$$EI\frac{\partial y^4(x,t)}{\partial x^4}+\rho A\frac{\partial y^2(x,t)}{\partial t^2}=f(x,t) \quad (1)$$

where E = Young's modulus, I = moment of inertia, ρ = density, A = beam cross section area with the initial condition

$$y(x,0)=\dot{y}(x,0)=0$$

and the boundary condition

$$\lim_{|x|\to\infty}\frac{\partial^n y(x,t)}{\partial x^n}=0 \quad n=0,1,2,3$$

$$f(x,t)=\delta(x)\delta(t).$$

Then, the impulse response function for the strain of the beam will be (McGhie, 1990)

$$h_\varepsilon(x,t)=\frac{h}{2}\frac{1}{2m\sqrt{4\pi a}}\frac{1}{a\sqrt{t}}\sin\left(\frac{x^2}{4at}-\frac{\pi}{4}\right) \quad (2)$$

where m = mass per unit length, $a=\sqrt{(EI/m)}$, h = beam height. Equation (2) leads to an infinite value at the moment of impact. This result arises from the fact that the simple beam theory predicts an infinite velocity for waves of small wavelength. As a consequence, use of the Timoshenko beam will predict finite wave velocities, leading to a more accurate model. The equation of motion for the Timoshenko beam is

$$\begin{aligned} EI\Phi''+\kappa AG(y'-\Phi)-\rho I\ddot{\Phi}&=0\\ \rho A\ddot{y}-\kappa AG(y''-\Phi')&=0\end{aligned} \quad (3)$$

where Φ = deformation angle, κ = shear correction factor. The superscript *dot* and *prime* mean time and space domain derivatives, respectively. Then, the impulse response function for the Timoshenko beam with semiinfinite length can be obtained using the Laplace transform as follows:

$$\begin{aligned} h_\varepsilon(x^*,t^*)&=0 \quad 0<t<\frac{x}{C_1}\\ &=B_1\left[\int_0^b\frac{\phi_4(\rho)}{\rho\phi_5(\rho)}\cos(\rho t^*)\right.\\ &\quad\cosh[B\phi_4(\rho)x^*]\,d\rho \quad (4)\\ &\quad+\int_0^a\frac{-1}{\rho\phi_1(\rho)}\{\phi_3(\rho)\sin[B\phi_3(\rho)x^*]\\ &\quad\sinh[\rho t^*-B\phi_2(\rho)x^*]\\ &\quad+\phi_2(\rho)\cos[B\phi_3(\rho)x^*]\cosh[\rho t^*\\ &\quad\left.-B\phi_2(\rho)x^*]\}\,d\rho\right] \quad \frac{x}{C_1}<t<\frac{x}{C_2}\\ &=B_1\int_0^b\frac{\phi_4(\rho)}{\rho\phi_5(\rho)}\cos(\rho t^*)\\ &\quad\cosh[B\phi_4(\rho)x^*]\,d\rho \quad t>\frac{x}{C_2}\end{aligned}$$

where

$$t^*=\sqrt{(EA)/(\rho I)}\,t, \quad x^*=\sqrt{(A/I)}\,x,$$
$$C_1=\sqrt{E/\rho}, \quad C_2=\sqrt{\kappa G/\rho}.$$

This solution shows that waves caused by impact propagate through the beam according to propagation velocities C_1, C_2. Functions in the integrands and variables in the above equation are summarized in Appendix A. The impulse response function for deflection $h_y(x^*, t^*)$ can be obtained similarly as the result of Eq. (4). This result shows that the impulse response function for the Timoshenko beam has a finite value at the moment of impact, unlike the Euler–Bernoulli beam, and may be expected to lead to more realistic results.

In the analysis of an infinite beam, however, reflection at the boundary cannot be considered. Also, the solution for the Timoshenko beam is composed of an integral equation. This solution leads to good results for the specified point, but is troublesome elsewhere in the spatial domain. In order to make up for these disadvantages, we consider a numerical scheme in the time domain and use two results in combination as follows. First, define four variables, moment, shear force, angular velocity, and velocity for the equation of a Timoshenko beam:

$$M=EI\frac{\partial\Phi}{\partial x}, \quad Q=\kappa AG\left(\frac{\partial y}{\partial x}-\Phi\right),$$
$$v_\phi=\frac{\partial\Phi}{\partial t}, \quad v_y=\frac{\partial y}{\partial t}. \quad (5)$$

Then, the Timoshenko beam equation, Eq. (3), which is the 4th order partial differential equation of the deflection y, can be converted by using these four variables:

$$\frac{\partial M}{\partial x}-\rho I\frac{\partial v_\phi}{\partial t}+Q=0 \quad (6)$$

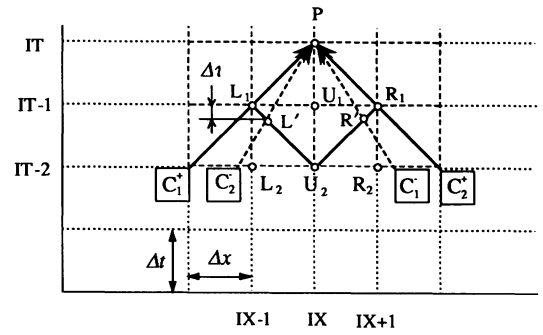

FIGURE 2 Formation of properties $\{s\}$ at point P.

$$\frac{\partial M}{\partial t} - EI\frac{\partial v_\phi}{\partial x} = 0 \tag{7}$$

$$\rho A\frac{\partial v_y}{\partial t} - \frac{\partial Q}{\partial x} = 0 \tag{8}$$

$$\frac{\partial Q}{\partial t} - \kappa AG\left(\frac{\partial v}{\partial x} - v_\phi\right) = 0. \tag{9}$$

Considering a characteristic path (Ames, 1977; Courant and Friedrichs, 1948) to change the direction of differentiation from the space and time coordinates to one parameter (Appendix B), and discretizing in the time and spatial domains (Fig. 2), we obtain the finite difference equations:

$$C_1^+;\ (M_{ix,it} - M_{ix-1,it-1}) - \rho IC_1(v_{\phi_{ix,it}} - v_{\phi_{ix-1,it-1}}) = -\frac{Q_{ix,it} + Q_{ix-1,it-1}}{2} C_1\Delta t \tag{10}$$

$$C_1^-;\ (M_{ix,it} - M_{ix-1,it-1}) + \rho IC_1(v_{\phi_{ix,it}} - v_{\phi_{ix-1,it-1}}) = +\frac{Q_{ix,it} + Q_{ix-1,it-1}}{2} C_1\Delta t \tag{11}$$

$$C_2^+;\ (Q_{ix,it} - Q_{L'}) - \rho AC_2(v_{y_{ix,it}} - v_{y_{L'}}) = -\frac{v_{\phi_{ix,it}} + v_{\phi_{L'}}}{2} \kappa AG(\Delta t + \Delta t) \tag{12}$$

$$C_2^-;\ (Q_{ix,it} - Q_{R'}) + \rho AC_2(v_{y_{ix,it}} - v_{y_{R'}}) = -\frac{v_{\phi_{ix,it}} + v_{\phi_{R'}}}{2} \kappa AG(\Delta t + \Delta t). \tag{13}$$

Table 1. Properties at Boundary

B.C.	Properties
Simple condition	Moment $M = 0$ velocity $v_y = 0$
Free condition	Moment $M = 0$ shear force $Q = 0$
Fixed condition	Velocity $v_y = 0$ ang. velocity $v_\phi = 0$

The subscript ix, it mean spatial and time domain mesh, respectively. Properties at points L' and R' can be obtained by linear interpolation with those of points L_1, L_2, R_1, R_2, U_1, and U_2 in Fig. 2. Then the above difference equations can be expressed in the matrix form

$$[W]\{s\}_{ix,it} = [RD1]\{s\}_{ix-1,it-1} + [RD2]\{s\}_{ix-1,it-2} + [LD1]\{s\}_{ix+1,it-1} + [LD2]\{s\}_{ix+1,it-2} + [UD1]\{s\}_{ix,it-1} + [UD2]\{s\}_{ix,it-2} \tag{14}$$

where $\{s\} = [M \quad v_\phi \quad Q \quad v_y]^T$. The component of matrices in Eq. (14) are summarized in Appendix C. Using this relation, properties $\{s\}$ at ix and it in the impacted beam can be obtained. Propagating through the beam as waves, these properties reach the boundary and it reflects corresponding to the nature of the boundary conditions.

For three kinds of boundary conditions, which are normally modeled, corresponding properties are determined as expressed in Table 1. Two additional properties at the boundary can be obtained using Eq. (15), which are affected by rightward moving waves as shown in Fig. 3:

$$[W]\{s\}_{ix,it} = [RD1]\{s\}_{ix-1,it-1} + [RD2]\{s\}_{ix-1,it-2} + [UD1]\{s\}_{ix,it-1} + [UD2]\{s\}_{ix,it-2}. \tag{15}$$

Because all properties at the boundary are known, reflection at the boundary can be realized using a numerical scheme. This effect is shown in Fig. 4, in which standing waves in the beam are developed as a consequence of reflected waves from the fixed boundary located at the position of $0.1L$. In order to obtain the impulse response function for any point, the Laplace transformed results, that is, responses for the external force $\delta(t)$, are used as the input conditions in the nu-

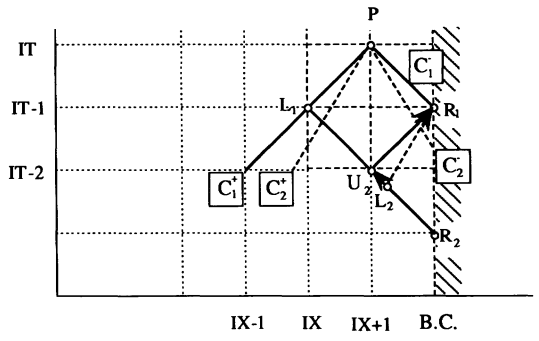

FIGURE 3 Formation of properties $\{s\}$ at boundary.

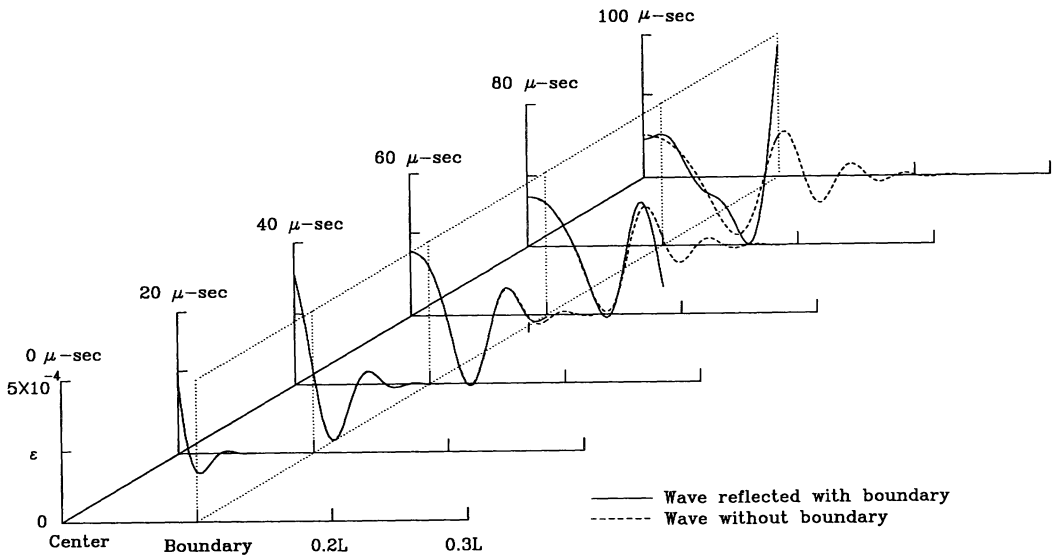

FIGURE 4 Reflection of the strain wave at fixed boundary.

merical scheme. Then, the impulse response function for an arbitrary point can be determined. The above scheme is applicable to an arbitrary boundary condition, that is, a time varying boundary.

RECONSTRUCTION OF IMPACT FORCE

Previously, the impulse response function has been developed by using the Laplace transform and a numerical scheme. Using these relations, the response at point x_0 of the beam for an impact force applied at x_i can be obtained using the convolution operator (*)

$$\begin{aligned} y(x_0, t) &= h_y(x_0 - x_i, t) * f(x_i, t) \\ \varepsilon(x_0, t) &= h_\varepsilon(x_0 - x_i, t) * f(x_i, t). \end{aligned} \tag{16}$$

If the point of input and measurement are known, then Eq. (16) can be written as

$$\begin{aligned} y_m(t) &= h_y(t) * f(t) \\ \varepsilon_m(t) &= h_\varepsilon(t) * f(t). \end{aligned} \tag{17}$$

The subscript m means the measured value. The deflection of a beam is negligibly small during the time of impact. Thus the measured strain signal will be used to find the unknown force $f(t)$ by deconvolution. In the case of the steady-state response, the ill-conditioning problems are frequently encountered in a deconvolution approach (Hillary and Ewins, 1984). But these are not critical problems in this impact case, in which the normal mode is not fully developed. It is known that results in the time domain approach are insensitive to data length and the position of the recording window (Chang and Sun, 1989). The reconstruction of the impact force is processed in the time domain. Define mean square error as

$$\text{error} = \sum_{i=0}^{N} \{[\varepsilon_m(i) - \tilde{\varepsilon}(i)]^2 + w_i \tilde{f}(i)^2\} \tag{18}$$

where w_i are weighting factors for strain and force. Then, $\tilde{f}(i)$ for minimizing error can be obtained as follows:

$$\begin{Bmatrix} \tilde{f}(0) \\ \tilde{f}(1) \\ \vdots \\ \tilde{f}(n) \end{Bmatrix} = \begin{bmatrix} \sum_{i=0}^{n} h_\varepsilon(i)^2 + 2w_0 & & & \\ r_{h_\varepsilon h_\varepsilon}(1) & \sum_{i=0}^{n-1} h_\varepsilon(i)^2 + 2w_1 & & \\ \vdots & \vdots & \ddots & \\ r_{h_\varepsilon h_\varepsilon}(n) & \cdots & \cdots & h_\varepsilon(0)^2 + 2w_n \end{bmatrix}^{-1} \begin{Bmatrix} r_{h_\varepsilon \varepsilon_m}(0) \\ r_{h_\varepsilon \varepsilon_m}(1) \\ \vdots \\ r_{h_\varepsilon \varepsilon_m}(n) \end{Bmatrix} \tag{19}$$

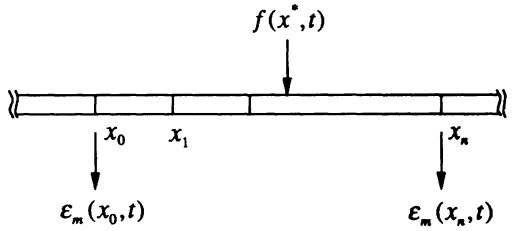

FIGURE 5 Arbitrary impact and measurement point.

where

$$r_{h_\varepsilon \varepsilon_m}(i) = \sum_{j=i}^{n} \varepsilon_m(j) h_\varepsilon(n-j).$$

If we consider the arbitrary impact case, then we can find the position and time history of the impact force by measuring strain at two points x_0, x_n (Fig. 5). Measurement set $\bar{\varepsilon}_m(x_0, t)$ using the measured strain $\varepsilon_m(x_0, t)$ at point x_0 and the recording window is prepared. Then the impact point $\tilde{x}^*$ is assumed successively from x_0 to x_n. The expected impact force $\tilde{f}(\tilde{x}^*, t)$ can be obtained by using Eq. (19). It is possible to generate the expected strain $\tilde{\varepsilon}_m(x_n, t)$ at x_n using the predetermined force $\tilde{f}(\tilde{x}^*, t)$. Compare the expected result with the measured result by introducing a normalized error as follows:

$$\text{error} = \sqrt{\frac{\sum_i [\tilde{\varepsilon}(x_n, t_i) - \bar{\varepsilon}_m(x_n, t_i)]^2}{\sum_i \bar{\varepsilon}_m^2(x_n, t_i)}} \quad (20)$$

where

$$\tilde{\varepsilon}(x_n, t) = h_\varepsilon(x_n - \tilde{x}^*, t) * \tilde{f}(\tilde{x}_n^*, t).$$

By plotting the above error, the impact position and shape of the impact force can be found. These procedures are summarized in the flow chart as shown in Fig. 6.

EXPERIMENTS AND NUMERICAL RESULTS

In order to test the validity of the response and force analysis, experiments and simulation were performed on a clamped–clamped beam as shown in Fig. 1. Strain gauges were attached to the bottom side of the beam for measuring the

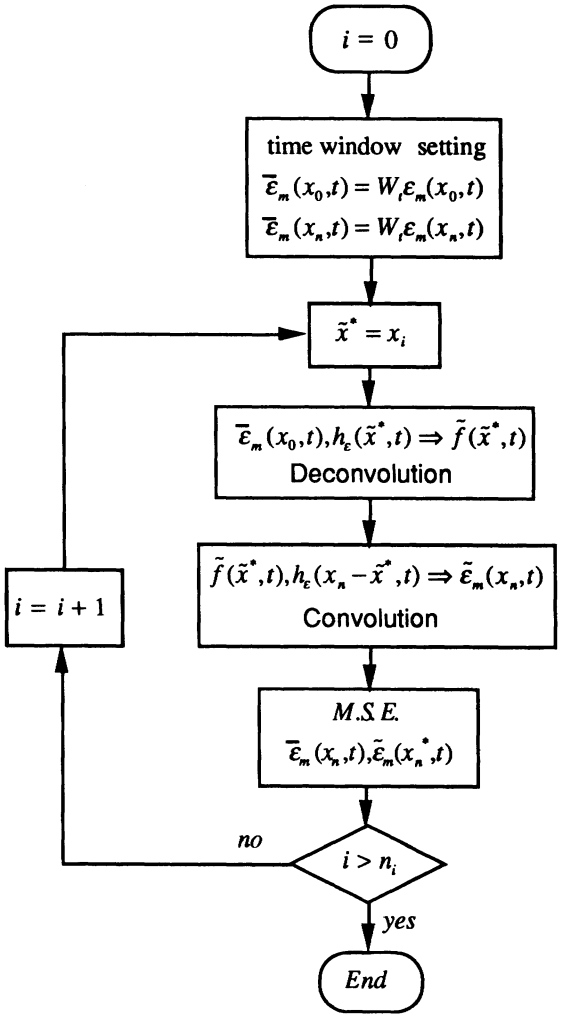

FIGURE 6 Flow chart of the simulation for an arbitrary impact.

bending strains. The experimental apparatus (Fig. 7) included a dynamic strain amplifier, which performs up to 200 kHz, an impact hammer and a force transducer, and a digital oscilloscope.

In order to observe the characteristics of an

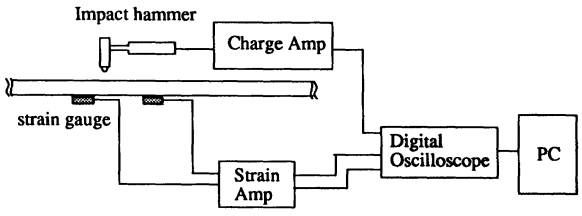

FIGURE 7 Measurement set-up.

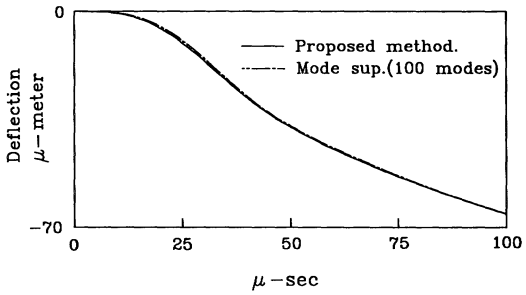

FIGURE 8(a) Deflection of impact point.

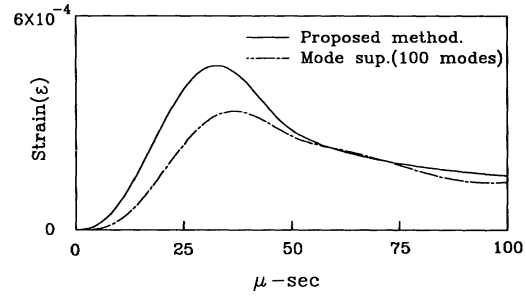

FIGURE 8(b) Strain history of impact point.

impact response, select the standard input as a squared half sine function with a magnitude of 1 kN, whose time duration (50 μs) is the same as that of a drop test of a steel ball. It has frequency component up to 100 kHz. The response of an impacted beam is solved with the mode superposition method, which is generally used in dynamics including impact problems, and its results are compared with those obtained by using the proposed algorithm. The responses at the center of beam are plotted in Fig. 8 for a given input. It is difficult to obtain the normal modes for the Timoshenko beam equation up to very high frequency. Thus, we use the results of the Euler–Bernoulli beam equation as many former researchers do. It can be seen from this figure that the normal mode solution with 100 modes (up to 116 kHz) summation for strain is not close to the numerical result. On the other hand, there is good correspondence for the deflection. Because the displacement of the beam converges better than the strain in the normal mode approach, if an accurate force contact model applicable in the wide frequency range is available, then the results of the analysis become more accurate. But we cannot reconstruct an impact force that will be used to obtain the force contact model because the displacement is a small quantity and difficult to measure during impact. The overall response of the beam for a given input is shown in Fig. 9. During impact, the strain in the vicinity of the impact site appears as sharp peaks and propagates through the beam. This result shows that the response of an impacted point that is not near the boundary is not affected by reflection from the boundary.

In order to validate the impulse response function determined previously, the input force and output strain are measured using an impact hammer and a strain gauge. It is shown in Fig. 10 that

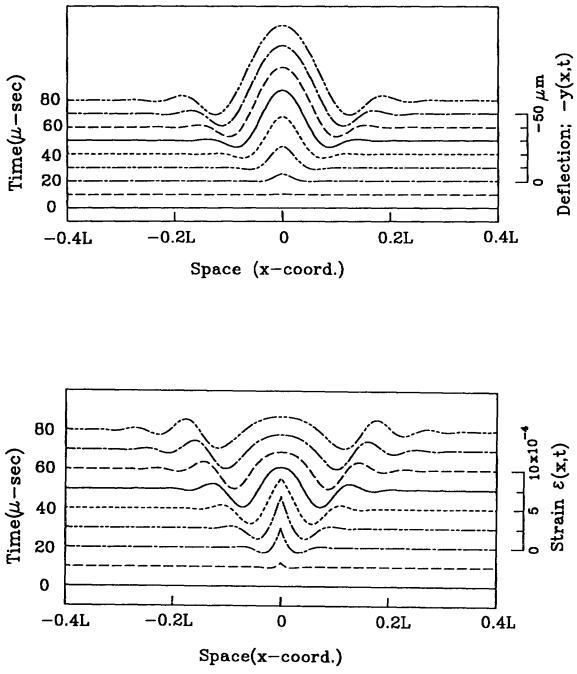

FIGURE 9 Beam response for the simulation input in the time and space domain: (a) deflection shape; (b) strain shape.

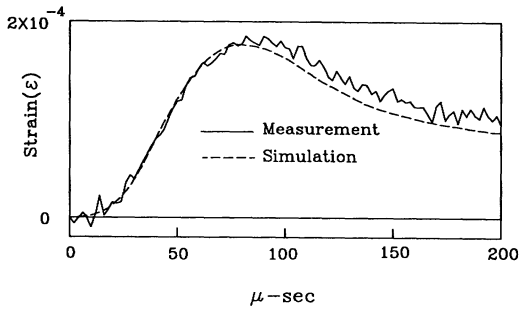

FIGURE 10 Measured and simulated strain history at impact point.

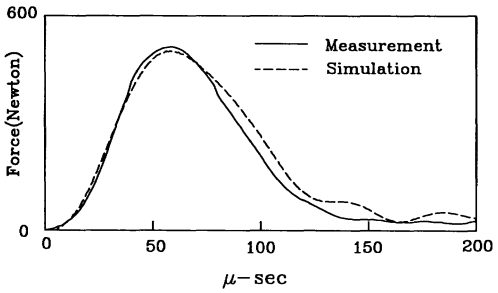

FIGURE 11 Measured and simulated force history at impact point.

results of the convolution with measured input forces matches well with the measured strain at the impact point. The recovered impact force by using a measured strain is also in good agreement with the measured one as shown in Fig. 11. Thus, it can be maintained from the above results that the response and force analyses are accurate.

Drop tests were implemented by striking the beam at the center with a steel ball with a diameter of 18.9 mm dropping from the heights of 0.25 m. The same experiments were repeated by varying the dropping height to 0.5 and 1.0 m. Instead of measuring the impact force, which is difficult to accomplish, the time duration of the impact was measured by using an electrical loop with a ball and beam and then compared with that of the recovered force as an indirect measure. The recovered forces are compared with the result using Hertz's contact theory (Fig. 12). As the drop height is increased, the impact force increases, and the recovered force varies more, which is different from the results using Hertz's contact theory. It may be due to the fact that Hertzian elastic contact theory is not applicable because local plastic deformation occurs at the center of

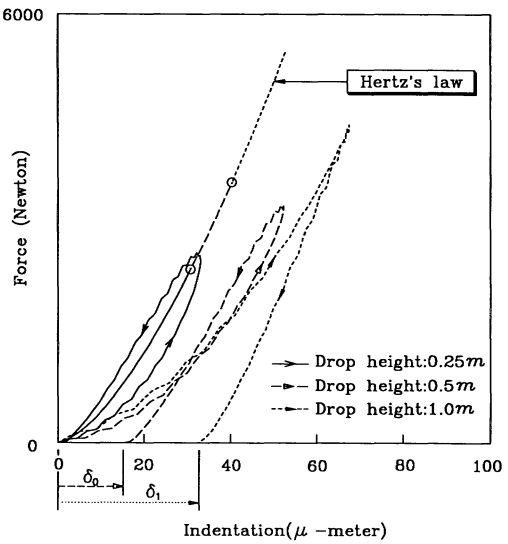

FIGURE 13 Indentation and force relations. δ_0, δ_1: Permanent deformation

the contact zone. To investigate this phenomenon, these results are plotted in a different way, that is, the forces are plotted with the variation of indentation, which is the difference of the displacements between a steel ball and the beam, for the loading and unloading (Fig. 13). The experimental result shows that as the drop height is increased, the amount of permanent deformation after unloading is significantly increased and the slope of this curve varies more from that of the Hertzian results. From this result, Hertz's contact theory needs to be modified according to the impact condition.

In order to verify the algorithm for finding the position and time history of an arbitrary impact case, a steel ball with diameter of 18.9 mm is dropped at x = 3 cm and strains are measured at

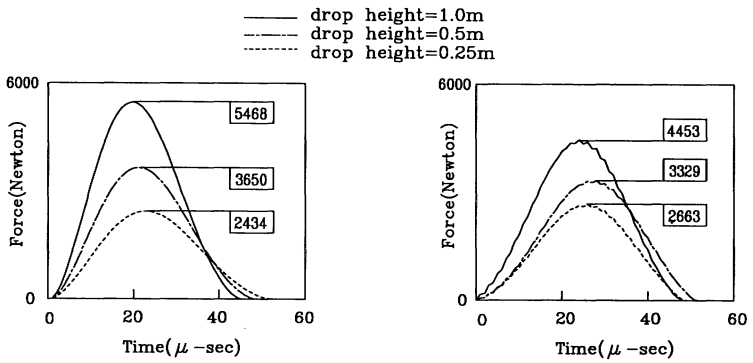

FIGURE 12 Reconstructed impact force in drop test (ball dia. = 18.9 mm). (a) Hertz's contact law; (b) proposed method.

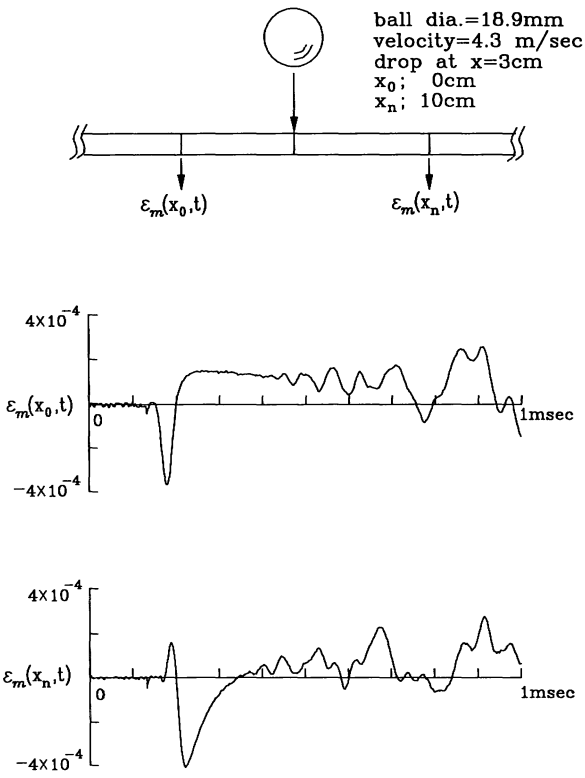

FIGURE 14 Test result of steel ball drop. (a) Configuration of drop test; (b) strain at $x_0 = 0$ cm; (c) strain at $x_n = 10$ cm.

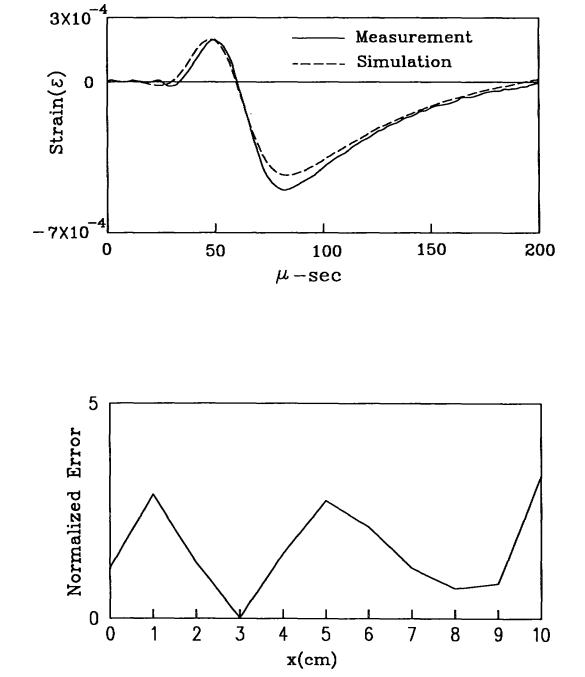

FIGURE 15 Simulated result of steel ball drop. (a) Strain history at $x_n = 10$ cm; (b) error plot.

$x = 0$ and 10 cm as shown in Fig. 14. Figure 15 shows that the resulting error has minimum value at $x = 3$ cm, where impact actually occurs. Because the impact force cannot be measured in this case, the convolution result from the recovered force and the impulse response function between the predicted impact point and the measured point, $x = 10$ cm, is compared with the measured signal at $x = 10$ cm (Fig. 15). From these results it is concluded that the suggested algorithm matches well with the measurements.

CONCLUSION

A method was presented for the transient response analysis of an impacted beam by using the impulse response function obtained using a Laplace transform and a numerical scheme considering reflection at the boundary. For this analysis, a beam was modeled as a Timoshenko beam, which seems to lead to more physically acceptable results. Using this relation, both the response and force analyses can be executed. From these results, it is concluded that there is good agreement between experimental and simulation results. From the drop test of a steel ball, the force was compared with Hertz's contact theory and some limitations of Hertz's contact law were discussed. For the analysis of an arbitrary impact, the proposed algorithm for finding the position and time history of the impact force was also carried out and from the results, it is maintained that the algorithm is sound.

REFERENCES

Ames, W. F., 1977, *Numerical Method For Partial Differential Equation,* 2nd ed., Academic Press, Boston.

Bateman, V. I., and Carne, T. G., 1991, "Force Reconstruction for Impact Tests," *Journal of Vibration and Acoustics,* ASME, Vol. 113, pp. 192–200.

Bateman, V. I., and Carne, T. G., 1992, "Force Reconstruction for Impact Tests of an Energy-Absorbing Nose," *International Journal of Analysis and Experimental Modal Analysis,* Vol. 7, pp. 41–50.

Cawley, P., and Clayton, D. L. R., 1987, "A Vibration Technique for the Measurement of Contact Stiffness, *MSSP,* Vol. 1, pp. 273–283.

Chang, C., and Sun, C. T., 1989, "Determining Transverse Impact Force on a Composite Laminates by Signal Deconvolution," *Experimental Mechanics,* Vol. 29, No. 4, pp. 414–419.

Courant, R., and Friedrichs, K. O., 1948, *Supersonic Flow and Shock Wave,* Interscience Publishers, Inc., New York.

Doyle, J. F., 1984a, "An Experimental Method for Determining the Dynamic Contact Law," *Experimental Mechanics,* Vol. 24, No. 1, pp. 10–16.

Doyle, J. F., 1984b, "Further Developments in Determining the Dynamic Contact Law," *Experimental Mechanics,* Vol. 24, No. 4, pp. 265–270.

Doyle, J. F., 1987, "Determining the Contact Force During the Transverse Impact of Plates," *Experimental Mechanics,* Vol. 27, No. 1, pp. 68–72.

Doyle, J. F., 1991, "Force Identification from Dynamic Response of Bi-Material Beams," DE-Vol. 36, *Machinery Dynamics and Element Vibration,* ASME, pp. 113–117.

Doyle, J. F., and Kamle, S., 1985, "An Experimental Study of the Reflection and Transmission of Flexural Waves at Discontinuities," *Journal of Applied Mechanics,* ASME, Vol. 52, pp. 669–673.

Doyle, J. F., and Kamle, S., 1987, "An Experimental Study of the Reflection and Transmission of Flexural Waves at an Arbitrary T-Joint," *Journal of Applied Mechanics,* ASME, Vol. 54, pp. 136–140.

Hillary, B., and Ewins, D. J., 1984," "The Use of Strain Gauges in Force Determination and Frequency Response Measurement," *Proceedings of Second International Modal Analysis Conference,* Orlando, FL, February 1984, pp. 627–634.

Hollandsworth, P. E., and Busby, H. R., 1989, "Impact Force Identification Using the General Inverse Technique," *International Journal Impact Engineering,* Vol. 8, pp. 315–322.

Leung, R. C. N., and Pinnington, R. J., 1990, "Wave Propagation Through Right-Angled Joint With Compliance-Flexural Incidence Wave," *Journal of Sound and Vibration,* Vol. 142, pp. 31–46.

Leung, R. C. N., and Pinnington, R. J., 1992, "Wave Propagation Through Right-Angled Joint With Compliance: Longitudinal Incidence Wave," *Journal of Sound and Vibration,* Vol. 153, pp. 223–237.

McGhie, R. D., 1990, "Flexural Wave Motion in Infinite Beam," ASCE, *Journal of Engineering Mechanics,* Vol. 116, No. 3, pp. 531–548.

Rizzi, S. A., and Doyle, J. F., 1992, "Spectral Analysis of Wave Motion in Plane Solids With Boundaries," *Journal of Vibration and Accoustics,* ASME, Vol. 114, pp. 133–140.

Stadler, W., and Shreeves, R. W., 1970, "The Transient and Steady-State Response of The Infinite Bernoulli–Euler Beam With Damping and an Elastic Foundation," *Quarterly Journal Mechanics and Applied Mathematics,* Vol. 23, pp. 197–208.

Willis, J. R., 1966, "Hertzian Contact of Anisotropic Bodies," *Journal Mechanics Solids,* Vol. 14, pp. 163–176.

Yamamoto, S., Sato, K., and Koseki, H., 1990, "A Study on Lateral Impact of Timoshenko Beam," *Computational Mechanics,* Vol. 6, No. 2, pp. 101–108.

APPENDIX A: INTEGRAND IN IMPULSE RESPONSE FUNCTION OF TIMOSHENKO BEAM

Functions in the integrands and variables in Eq. (4) are as follows

$$\phi_1(\rho) = \sqrt{a^2 - \rho^2} \tag{A.1}$$

$$\phi_2(\rho) = \sqrt{\frac{\rho + \frac{1}{\chi + 1}\sqrt{4\chi\rho^2 + (\chi - 1)^2 a^2}}{2}}$$

$$\phi_3(\rho) = \sqrt{\frac{-\rho + \frac{1}{\chi + 1}\sqrt{4\chi\rho^2 + (\chi - 1)^2 a^2}}{2}}$$

$$\phi_4(\rho) = \sqrt{\left(\frac{\chi - 1}{\chi + 1}\right)\phi_5(\rho)\rho - \rho^2}$$

$$\phi_5(\rho) = \sqrt{a^2 + \rho^2}$$

$$C_1 = \sqrt{\frac{E}{\rho}}, \quad C_2 = \sqrt{\frac{\kappa G}{\rho}}, \quad \chi = \frac{C_1}{C_2}$$

$$a = \sqrt{\frac{2C_2}{C_1 - C_2}}, \quad b = \sqrt{\frac{C_2}{C_1}}$$

$$B = \sqrt{\frac{C_1 + C_2}{2C_2}}, \quad B_1 = \frac{h}{2}\frac{aB}{\pi\chi}, \quad h = \text{beam height}$$

APPENDIX B: COORDINATE TRANSFORMATION

A linear combination $a[\partial M(x, t)/\partial x] + b[\partial M(x, t)/\partial t]$ of the two derivatives of a function $M(x, t)$ is defined by derivative of M in a direction given by $dx : dt = a : b$. If $\chi(\sigma)$, $t(\sigma)$ represents a curve with $(\partial x/\partial\sigma) : (\partial x/\partial\sigma) = a : b$, then $a[\partial M(x, t)/\partial x] + b[\partial M(x, t)/\partial t]$ is a derivative of M along this curve. We express Eqs. (6) and (7) using linear operators L_1, L_2 and consider another linear combination (B.1) so that the derivatives in L combine with derivatives in the same direction.

$$\begin{aligned} L &= \lambda_1 L_1 + \lambda_2 L_2 \\ &= \lambda_1 \frac{\partial M}{\partial x} + \lambda_2 \frac{\partial M}{\partial t} - \lambda_2 EI \frac{\partial \omega}{\partial x} \\ &\quad - \lambda_1 \rho I \frac{\partial \omega}{\partial t} + \lambda_1 Q = 0. \end{aligned} \tag{B.1}$$

If the direction is given by $x(\sigma)$, $t(\sigma)$ as above, then the condition is

$$\lambda_1 : \lambda_2 = -\lambda_2 EI : -\lambda_1 \rho I = \frac{\partial x}{\partial\sigma} : \frac{\partial t}{\partial\sigma}. \tag{B.2}$$

After multiplication of Eq. (B.1) by x_σ and t_σ [$x_\sigma = (\partial x/\partial\sigma)$, $t_\sigma = (\partial t/\partial\sigma)$] and using the results of Eqs. (B.1), (B.2) can be expressed in matrix form:

$$\begin{bmatrix} t_\sigma & x_\sigma \\ \rho I x_\sigma & -EI t_\sigma \\ \dfrac{\partial M}{\partial\sigma} + Q x_\sigma & -EI\dfrac{\partial\omega}{\partial\sigma} \\ -\rho I\dfrac{\partial\omega}{\sigma t} + Q t_\sigma & \dfrac{\partial M}{\partial\sigma} \end{bmatrix} \begin{Bmatrix} \lambda_1 \\ \lambda_2 \end{Bmatrix} = \begin{Bmatrix} 0 \\ 0 \\ 0 \\ 0 \end{Bmatrix}. \quad \text{(B.3)}$$

If λ_1, λ_2 in Eq. (B.3) have a nontrivial solution, the condition, which is a characteristic relation, is

$$\frac{x_\sigma}{t_\sigma} = \pm\sqrt{\frac{E}{\rho}} = \pm C_1. \quad \text{(B.4)}$$

As a result, a linear operator in (B.1) can be expressed in Eqs. (9) and (10). Similarly, for Eqs. (8) and (9), the condition is

$$\frac{x_\sigma}{t_\sigma} = \pm\sqrt{\frac{\kappa G}{\rho}} = \pm C_2 \quad \text{(B.5)}$$

and the results are Eqs. (12) and (13).

APPENDIX C: COMPONENTS OF MATRICES

Matrices in Eq. (14) are as follows:

$$[W] = \begin{bmatrix} 1 & -\rho I C_1 & \dfrac{C_1\Delta t}{2} & 0 \\ 1 & \rho I C_1 & -\dfrac{C_1\Delta t}{2} & 0 \\ 0 & \dfrac{\kappa AG}{2}(2-\beta)\Delta t & 1 & -\rho A C_2 \\ 0 & \dfrac{\kappa AG}{2}(2-\beta)\Delta t & 1 & \rho A C_2 \end{bmatrix}$$

$$[RD1] = \begin{bmatrix} 1 & -\rho I C_1 & -\dfrac{C_1\Delta t}{2} & 0 \\ 0 & 0 & 0 & 0 \\ 0 & \dfrac{\kappa AG}{2}(2-\beta)\beta^2\Delta t & \beta^2 & -\rho A C_2\beta^2 \\ 0 & 0 & 0 & 0 \end{bmatrix}$$

$$[RD2] = \begin{bmatrix} 0 & 0 & 0 & 0 \\ 0 & 0 & 0 & 0 \\ 0 & -\dfrac{\kappa AG}{2}(2-\beta)\beta(1-\beta)\Delta t & \beta(1-\beta) & -\rho A C_2\beta(1-\beta) \\ 0 & 0 & 0 & 0 \end{bmatrix}$$

$$[LD1] = \begin{bmatrix} 0 & 0 & 0 & 0 \\ 1 & \rho I C_1 & \dfrac{C_1\Delta t}{2} & 0 \\ 0 & 0 & 0 & 0 \\ 0 & \dfrac{\kappa AG}{2}(2-\beta)\beta^2\Delta t & \beta^2 & \rho A C_2\beta^2 \end{bmatrix}$$

$$[LD2] = \begin{bmatrix} 0 & 0 & 0 & 0 \\ 0 & 0 & 0 & 0 \\ 0 & 0 & 0 & 0 \\ 0 & -\dfrac{\kappa AG}{2}(2-\beta)\Delta t & 1 & \rho A C_2 \end{bmatrix}$$

$$[UD1] = [RD2] + [LD2]$$

$$[UD2] = \begin{bmatrix} 0 & 0 & 0 & 0 \\ 0 & 0 & 0 & 0 \\ 0 & -\frac{\kappa AG}{2}(2-\beta)(1-\beta^2)\Delta t & (1-\beta^2) & -\rho AC_2(1-\beta^2) \\ 0 & -\frac{\kappa AG}{2}(2-\beta)(1-\beta^2)\Delta t & (1-\beta^2) & \rho AC_2(1-\beta^2) \end{bmatrix}$$

$$\beta = \frac{2C_2}{C_1 + C_2} \quad 0 < \beta < 1.$$